

Received November 1, 2016, accepted November 8, 2016., date of publication November 22, 2016, date of current version December 8, 2016.

Digital Object Identifier 10.1109/ACCESS.2016.2628407

# Facial Emotion Recognition Based on Biorthogonal Wavelet Entropy, Fuzzy Support Vector Machine, and Stratified Cross Validation

YU-DONG ZHANG<sup>1,2,3</sup>, ZHANG-JING YANG<sup>1</sup>, HUI-MIN LU<sup>4</sup>, XING-XING ZHOU<sup>2</sup>,  
PREETHA PHILLIPS<sup>5,6</sup>, QING-MING LIU<sup>7</sup>, AND SHUI-HUA WANG<sup>2</sup>

<sup>1</sup>School of Technology, Nanjing Audit University, Nanjing 211815, China

<sup>2</sup>School of Computer Science and Technology, Nanjing Normal University, Nanjing 210023, China

<sup>3</sup>Department of Electrical Engineering, The City College of New York, New York, NY 10031, USA

<sup>4</sup>Department of Mechanical and Control Engineering, Kyushu Institute of Technology, Fukuoka 804-8550, Japan

<sup>5</sup>School of Natural Sciences and Mathematics, Shepherd University, Shepherdstown, WV 25443, USA

<sup>6</sup>West Virginia School of Osteopathic Medicine, Lewisburg, WV 24901, USA

<sup>7</sup>School of Psychology, Nanjing Normal University, Nanjing 210023, China

Corresponding author: Y.-D. Zhang (zhangyudong@njnu.edu.cn), Z.-J. Yang (yzzjjj@126.com), and S.-H. Wang (wangshuihua@njnu.edu.cn)

This work was supported in part by NSFC under Grant 61602250, Grant 61503195, Grant 61462064, Grant 61203243, Grant 61402231, Grant 61603192, and Grant 61272077, in part by the Natural Science Foundation of Jiangsu Province under Grant BK20150983 and Grant BK20161580, in part by the Program of Natural Science Research of Jiangsu Higher Education Institutions under Grant 16KJB520025, Grant 16KJB520020, Grant 15KJB470010, Grant 15KJB520018, and Grant 2KJA63001, in part by the Open Project Program of the State Key Laboratory of CAD&CG, Zhejiang University under Grant A1616, and in part by the Open Research Fund of Key Laboratory of Network Crime Investigation of Hunan Provincial Colleges under Grant 2015HNWLFZ058.

**ABSTRACT** Emotion recognition represents the position and motion of facial muscles. It contributes significantly in many fields. Current approaches have not obtained good results. This paper aimed to propose a new emotion recognition system based on facial expression images. We enrolled 20 subjects and let each subject pose seven different emotions: happy, sadness, surprise, anger, disgust, fear, and neutral. Afterward, we employed biorthogonal wavelet entropy to extract multiscale features, and used fuzzy multiclass support vector machine to be the classifier. The stratified cross validation was employed as a strict validation model. The statistical analysis showed our method achieved an overall accuracy of  $96.77 \pm 0.10\%$ . Besides, our method is superior to three state-of-the-art methods. In all, this proposed method is efficient.

**INDEX TERMS** Facial emotion recognition, facial expression, biorthogonal wavelet entropy, support vector machine, fuzzy logic.

## I. INTRODUCTION

Emotion recognition (ER) [1] studies how to identify human emotions, typically, the sources are facial expressions, and we call it as facial emotion recognition (FER) [2]. Academically, the facial expression denotes motions and positions of facial muscles beneath skin of the face. Those movements are a form of nonverbal communication, and convey the emotional status to an observer. The research of FER benefits a massive of fields, for example, the in-car conversational interface [3], EEG signal [4], the theatre performance [5], speech emotion recognition [6], bipolar disorder [7], adolescents with disabilities [8], depressive symptom [9], Parkinson's disease [10], etc.

There are various studies using various methods to solve the FER problems. Drume and Jalal [11] presented

a two-level classification approach, i.e., principal component analysis (PCA) at level 1 was boosted by support vector machine (SVM) at level 2. Vivek and Guddeti [12] combined cat swarm optimization (CSO), genetic algorithm (GA), and particle swarm optimization (PSO). This hybrid bio-inspired algorithm was in conjunction with SVM. Ali *et al.* [13] used radon transform (RT), higher-order spectral (HOS), and SVM. Takehara *et al.* [14] proposed to use a small-world network model. Alhussein [15] used multi-scale Weber local descriptor (MS-WLD) and SVM.

Nevertheless, the performances of above methods are not satisfying. Besides, their method cannot handle outliers and noises. In this study, our contribution is to propose a new FER system, which uses biorthogonal wavelet entropy as the feature detector. It combines the advantages of both

biorthogonal wavelet transform and Shannon entropy. Furthermore, a powerful variant of SVM, fuzzy SVM, was introduced to improve the performance of conventional SVM.

The structure of the remainder is organized as follows: Section II gives the materials used in this study, and presents the preprocessing method. Section III provides the methodology on feature extraction. Section IV describes the classification method. Section V contains the results and discussions. Finally, Section VI concludes the paper.

## II. SUBJECTS

We enrolled 20 subjects with ages from twenty to thirty-five by online advertisements. Each subject was requested to lay seven facial expressions (happy, sadness, surprise, anger, disgust, fear, and neutral). We photographed each facial expression of each subject ten times by Canon digital camera, and finally picked up five photos approved by three experienced psychologists. In the final, we have 700 images in total.

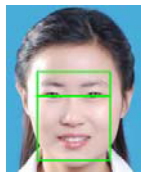


FIGURE 1. Face detection from a female face model.

Face detection method was used based on the face model shown in Figure 1. Suppose the distance between two centers of eyes be  $D$ , we have the geometric face model rules [16] as follows: (i) Width of the mouse is  $D$ . (ii) Width of nose is  $0.8D$ . (iii) Vertical distance between eyes and center of mouth is  $D$ . (iv) Vertical distance between eyes and center of nostril is  $0.6D$ . (v) Vertical distance between eyes and eyebrows is  $0.4D$ . To cover the whole face, we extend  $0.4D$  in both upper and lower margin, and  $0.4D$  in both left and right margins. Finally, we get a photo image with size of width of  $1.8D$  and height of  $2.2D$ . Figure 2 shows the seven emotional expressions of both a male and a female faces.

## III. FEATURE EXTRACTION

### A. DISCRETE WAVELET TRANSFORM

Signal processing has gone through three important generations as shown in Figure 3. For the first generation, Fourier transform (FT) decomposes the signal into its frequencies (as the music chord). Then, the second generation analyze local sections of signal, and the famous technique is short time FT (ST-FT). In the third generation, the wavelet transform (WT) used a variable-size window to analyze the signal in multi-scales [17]. In the past decade, the discrete WT (DWT) has been proven as one of the most efficient signal processing techniques, and applied in various fields, such as fault detection [18], JPEG 2000 [19], dendrite spine recognition [20], voltage signal feature extraction [21], QRS detection [22], etc.

Suppose we have a continuous signal  $x(t)$ , we then sample it at initial time  $t_0$  with interval  $\Delta t$ , and thus we get the

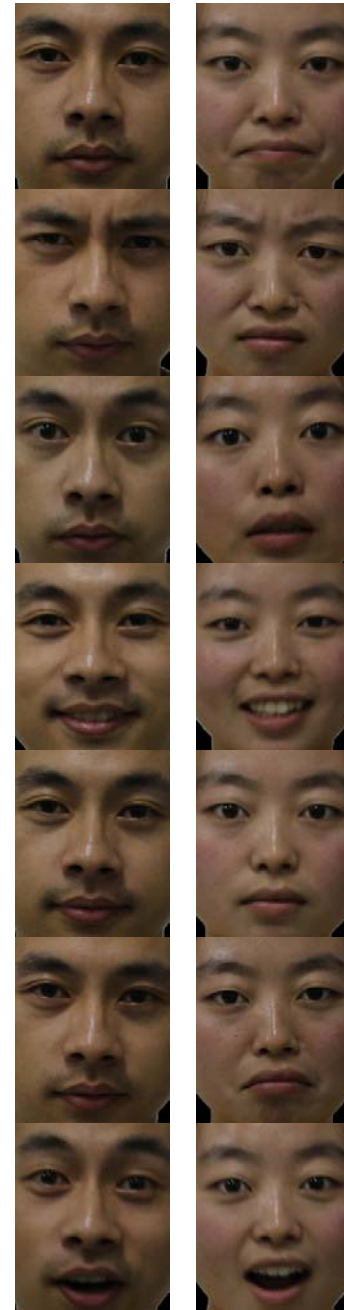


FIGURE 2. Samples of the dataset (The first column gives the seven emotion expressions of a male face, and the second column gives the seven emotion expressions of a female face).

discrete version of the continuous signal as

$$x(n) = x(t_0 + n\Delta t) \tag{1}$$

where  $n$  is in the range of integer set  $(0, 1, \dots, N - 2, N - 1)$ . To get the DWT results, we need to pass  $x(n)$  through a series of both low-pass filter  $l$  and high-pass filter  $k$ , and then downsampled by 2:

$$C_l(n) = \sum_{m=-\infty}^{+\infty} x(m) \times l(2n - m) \tag{2}$$

$$C_k(n) = \sum_{m=-\infty}^{+\infty} x(m) \times k(2n - m) \tag{3}$$

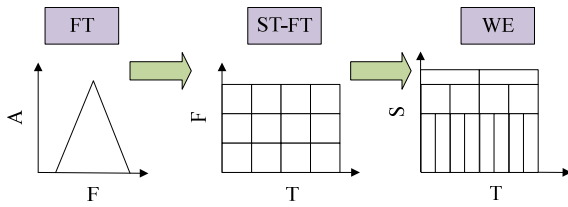


FIGURE 3. Three generations of signal processing.

Here  $m$  is a temporary variable. The coefficients  $C_l$  and  $C_k$  are also known as the approximation coefficient and detail coefficient. One level decomposition is finished till now. For multi-level decomposition, the approximation coefficient is decomposed further into its corresponding approximation and detail coefficient, as shown in Figure 4.

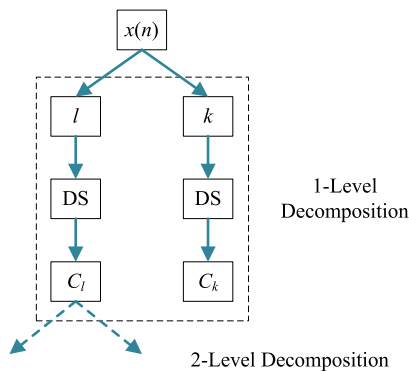


FIGURE 4. Illustration of DWT (DS represents a 2x downsampling operation).

Note that for 2D image processing, we do not use  $C_l$  and  $C_k$  to represent the coefficient subbands of each decomposition. Instead, we have four coefficient subbands at each level, since the low-pass filter and high-pass filter will be used at both horizontal and vertical directions. Following standard convention, we used  $C_a, C_h, C_v,$  and  $C_d$  to denote these four coefficient subbands.

**B. BIORTHOGONAL WAVELET ENTROPY**

Two shortcomings exist for using DWT to extract features from face expression images. First, the traditional wavelet suffers from complicated calculation. Second, the DWT may yield too many features, which will hurdle the following classification.

To solve above two issues, we proposed two improvements. In the first improvement, we revisit the development of wavelet family as shown in Figure 5. We observe that wavelet transform was replaced with orthogonal wavelet transform (abbreviated as OWT), and OWT was recently replaced with biorthogonal wavelet transform (abbreviated as BWT).

Two advantages exist for OWT: (i) its associated wavelet transform is orthogonal [23], i.e., its inverse wavelet transform is the adjoint of the wavelet transform. (ii) OWT can be defined merely on the basis of the scaling filter [24] (i.e., the low-pass filter). BWT inherits the first

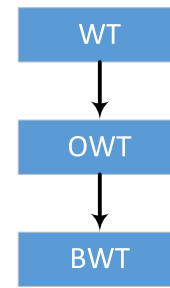


FIGURE 5. Development from WT to OWT to BWT (WT = wavelet transform, OWT = orthogonal wavelet transform; BWT = biorthogonal wavelet transform).

advantage of OWT [25], but its definition is based on both low-pass filter and high-pass filter. It has another advantage that it allows more degrees of freedom than OWT [26].

In the second improvement, we combined the Shannon entropy [27], [28] with BWT, and thus proposed a novel multiscale feature extraction technique named as biorthogonal wavelet entropy (BWE). The Shannon entropy was performed over each coefficient subband, which is regarded as a gray-level image. The Shannon entropy is implemented with following equation:

$$N(Y) = - \sum_{i=1}^L P(y_i) \log P(y_i) \tag{4}$$

Here  $Y$  is a coefficient subband.  $y_i$  is the  $i$ -th gray-level of  $Y$ .  $P$  represent the probability density function.  $L$  is the total number of gray-values.  $N$  is the entropy operation.

Figure 6 shows the block diagram of calculating a 2-level BWE. In the first step, a facial expression image was imported. Next, we performed 1-level BWT and obtained four coefficient subbands, i.e.,  $C_a(1), C_h(1), C_v(1),$  and  $C_d(1)$ . Here ( $j$ ) represents the  $j$ -level decomposition. In the third step, we performed a 2-level BWT, that means, we decomposed the  $C_a(1)$  into four higher-level subbands of  $C_a(2), C_h(2), C_v(2)$  and  $C_d(2)$ . Finally, the Shannon entropy in equation (4) was implemented over these seven coefficient subbands.

**IV. CLASSIFICATION**

**A. SUPPORT VECTOR MACHINE**

In the field of supervised learning, Support vector machine (SVM) is one of the most influential approaches. It has been successfully applied into identify brains [29], spatio-temporal activity [30], Alzheimer’s disease [31], online review [32], multiple sclerosis [33], etc. Suppose we have two classes of +1 and -1, and the dataset is

$$\{(p_n, t_n) | p_n \in \mathbb{R}^d\}, \quad n = 1, \dots, N \tag{5}$$

where  $N$  represents the number of samples,  $d$  is the dimension of input features,  $p_n$  is the feature vector of  $n$ -th sample data, and  $t_n$  is its corresponding target label.

$$t_n = \begin{cases} +1 & \text{class} = +1 \\ -1 & \text{class} = -1 \end{cases} \tag{6}$$

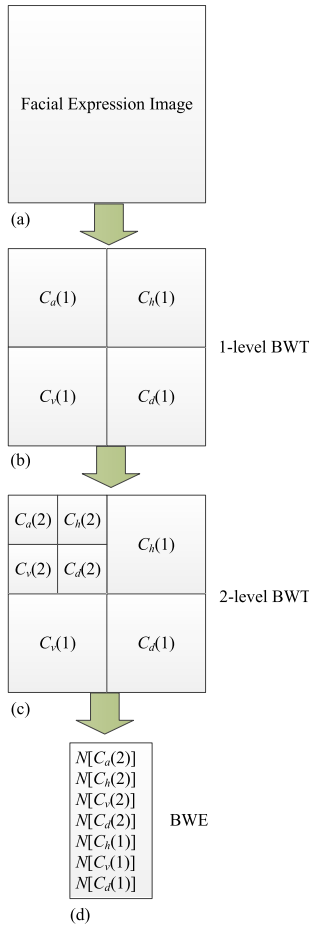


**FIGURE 6. Block Diagram of a 2-level BWE: (a) A facial expression image; (b) 1-level BWT; (c) 2-level BWT; (d) Shannon entropy calculation. In this figure, (j) represents the j-level decomposition.**

The aim of SVM is to create a hyperplane with dimension of  $(d-1)$ , which can separate the two classes. The model of SVM is similar to logistic regression, since both are driven by a linear function

$$\mathbf{w}^T p - b = 0 \tag{7}$$

which is also the form of the hyperplane to be created.  $\mathbf{w}$  and  $b$  have the similar physical meanings as in logistic function.  $\mathbf{w}$  means the weights and  $b$  means the bias. The mathematical solution of obtaining the  $\mathbf{w}$  and  $b$  are as follows:

$$\begin{aligned} \min_{\mathbf{w}, b} & \frac{1}{2} \|\mathbf{w}\|^2 \\ \text{s.t. } & t_n (\mathbf{w}^T p_n - b) \geq 1, \quad n = 1, \dots, N \end{aligned} \tag{8}$$

If the input features contain noises, we can use the “soft margin” technique. After adding the positive slack vector  $\rho = (\rho_1, \dots, \rho_n, \dots, \rho_N)$ , equation (8) is changed to:

$$\begin{aligned} \min_{\mathbf{w}, \rho, b} & \frac{1}{2} \|\mathbf{w}\|^2 + Le^T \rho \\ \text{s.t. } & \begin{cases} t_n (\mathbf{w}^T p_n - b) \geq 1 - \rho_n \\ \rho_n \geq 0 \end{cases}, \quad n = 1, \dots, N \end{aligned} \tag{9}$$

where  $e$  is a vector of ones of  $N$ -dimension, and  $L$  is the error penalty.

The constraint optimization problem in equation (9) is solved by the “Lagrange multiplier” technique as:

$$\begin{aligned} \min_{\mathbf{w}, \rho, b} \max_{\varphi, \gamma} & \left\{ \frac{1}{2} \|\mathbf{w}\|^2 + Le^T \rho \sum_{n=1}^N \varphi_n \left[ t_n (\mathbf{w}^T p_n - b) + \rho_n - 1 \right] \right. \\ & \left. - \sum_{n=1}^N \rho_n \gamma_n \right\} \end{aligned} \tag{10}$$

The *dual form* technique is used to solve equation (10), since the min-max problem is difficult to solve. In this way, we have:

$$\begin{aligned} \max_{\varphi} & \sum_{n=1}^N \varphi_n - \frac{1}{2} \sum_{n=1}^N \sum_{m=1}^N \varphi_m \varphi_n t_m t_n p_m^T p_n \\ \text{s.t. } & \begin{cases} L \geq \varphi_n \geq 0 \\ \sum_{n=1}^N t_n \varphi_n = 0 \end{cases}, \quad n = 1, \dots, N \end{aligned} \tag{11}$$

**B. MULTICLASS SVM**

Traditionally, SVMs were developed for two-class problem [34]. In this study, we need to handle a seven-class classification problem: happy, sadness, surprise, anger, disgust, fear, and neutral. Hence, we used the winner-takes-all (WTA) technique [35] to break the 7-class task into multiple 2-class tasks [36].

That means, we need to create 7 individual SVMs, each one was trained to detect one class from the remaining classes. For example, the first SVM will judge whether a new sample is Class 1 or not Class 1, the second SVM judges a new sample is Class 2 or not Class 2, etc. We label the seven individual SVMs as “1v1”, “2v2”, “3v3”, “4v4”, “5v5”, “6v6”, and “7v7”, respectively. Here “*ivi*” represents the corresponding individual SVM detect Class  $i$  from other classes (not Class  $i$ ).

A score  $S_k$  is associated with the output of  $k$ -th individual SVM “ $k$ v ~~$k$~~ ”. The class label set  $\mathcal{K}$  is defined as

$$\mathcal{K} = [1 \quad 2 \quad 3 \quad 4 \quad 5 \quad 6 \quad 7] \tag{12}$$

Finally, the final output of the combined classifier is

$$O(p) = \arg \max_{k \in \mathcal{K}} S_k(p) \tag{13}$$

Figure 7 shows the diagram of 7-class SVM using WTA. Here assume the score of each individual classifier is  $-0.2, 0.6, 0.5, -0.3, -0.8, 0.9$ , and  $-0.7$ , respectively. The argmax function outputs 6, i.e., the new facial expression image is identified as Class 6.

**C. FUZZY MEMBERSHIP FUNCTION**

The fuzzy logic [37] is introduced here, namely, we applies the fuzzy membership function (FMF) [38] to each training data. The original training data contains the input and target, and the fuzzy training data contains the input, the target,

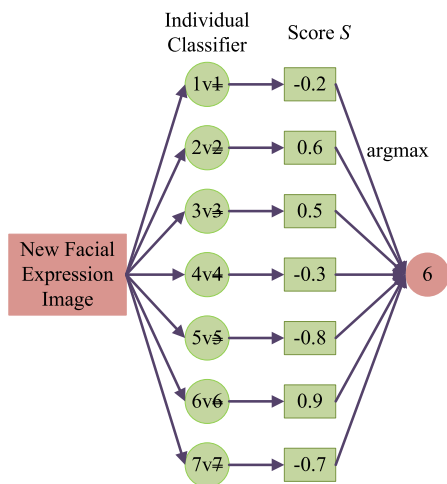


FIGURE 7. Diagram of a 7-class SVM using WTA technique.

and the fuzzy altitude. Mathematically, equation (5) is transformed to

$$\begin{cases} (p_n, t_n, a_{n,k}) | p_n \in \mathbb{R}^d \\ 0 < a_{n,k} \leq 1 \end{cases} \quad k = 1, 2, \dots, K, \quad n = 1, \dots, N \quad (14)$$

where  $a_{n,k}$  represents the fuzzy altitude [39] of sample  $p_n$  towards class  $t_n$  when training  $k$ -th individual classifier. Remember the two classes of  $k$ -th individual are defined as either  $+k$  or  $-k$ , viz., we have seven different fuzzy altitudes for each training data.

Suppose the mean of class  $+k$  is  $m_{+k}$ , and the mean of class  $-k$  is  $m_{-k}$ . Mathematically,

$$m_{+k} = \text{mean}_n (p_n | t_n = +k) \quad (16)$$

$$m_{-k} = \text{mean}_n (p_n | t_n = -k) \quad (17)$$

We can deduce the radius of Class  $+k$  and Class  $-k$  as:

$$r_{+k} = \max_{\{p_n: t_n = +k\}} |m_{+k} - p_n| \quad (18)$$

$$r_{-k} = \max_{\{p_n: t_n = -k\}} |m_{-k} - p_n| \quad (19)$$

The FMF is defined based on the means and radii of both classes

$$a_{n,k} = \begin{cases} 1 - |m_{+k} - p_n| / (r_{+k} + \nu) & t_n = +k \\ 1 - |m_{-k} - p_n| / (r_{-k} + \nu) & t_n = -k \end{cases} \quad (20)$$

Here  $\nu$  is a positive parameter, so as to guarantee the fuzzy altitude is greater than zero.

#### D. FUZZY MULTICLASS SVM

After definition of FMF in Section IV-C, we can arrive at the mathematical form of the individual FSVM. When  $k$ -th individual classifier is an FSVM, the two classes of processed dataset are defined as either  $+k$  or  $-k$ , assume vector  $\mathbf{a}$  is the membership vector of all data

$$a_k = (a_{1,k}, a_{2,k}, \dots, a_{n,k}, \dots, a_{N,k}) \quad (21)$$

We can draw the hyperplane of individual FSVM [40] as

$$\begin{aligned} \min_{\mathbf{w}, \rho, b} & \frac{1}{2} \|\mathbf{w}\|^2 + La_k^T \rho \\ \text{s.t.} & \begin{cases} t_n (\mathbf{w}^T p_n - b) \geq 1 - \rho_n \\ \rho_n \geq 0 \end{cases}, \quad n = 1, \dots, N \end{aligned} \quad (22)$$

A smaller  $a_{n,k}$  decreases the influence of the slack vector  $\rho_n$ , such that the corresponding sample  $p_n$  is regarded less substantial [41]. The Lagrangian [42] is obtained in a similar way as

$$\begin{aligned} \min_{\mathbf{w}, \rho, b} \max_{\varphi, \gamma} & \left\{ \frac{1}{2} \|\mathbf{w}\|^2 + La_k^T \rho - \sum_{n=1}^N \varphi_n [t_n (\mathbf{w}^T p_n - b) + \rho_n - 1] \right. \\ & \left. - \sum_{n=1}^N \rho_n \gamma_n \right\} \end{aligned} \quad (23)$$

The dual form is obtained as

$$\begin{aligned} \max_{\varphi} & \sum_{n=1}^N \varphi_n - \frac{1}{2} \sum_{n=1}^N \sum_{m=1}^N \varphi_m \varphi_n t_m t_n p_m^T p_n \\ \text{s.t.} & \begin{cases} 0 \leq \varphi_n \leq a_{n,k} L \\ \sum_{n=1}^N t_n \varphi_n = 0 \end{cases}, \quad n = 1, \dots, N \end{aligned} \quad (24)$$

#### E. MODEL VALIDATION

A 10-fold stratified cross validation was used to validate our model. Since the 700-image model contains 100 image for each emotion, the stratification splits the folds in the way that each fold contains the same distribution of emotion images as shown in Table 1.

TABLE 1. Stratification in cross validation.

Fold	Anger	Disgust	Fear	Happy	Neutral	Sadness	Surprise
I	10	10	10	10	10	10	10
II	10	10	10	10	10	10	10
III	10	10	10	10	10	10	10
IV	10	10	10	10	10	10	10
V	10	10	10	10	10	10	10
VI	10	10	10	10	10	10	10
VII	10	10	10	10	10	10	10
VIII	10	10	10	10	10	10	10
IX	10	10	10	10	10	10	10
X	10	10	10	10	10	10	10

Although SVM has closed-form solution, we used iterative gradient-based learning to train its weights and biases. This can bring us an advantage, that the training shall be stopped if the error on validation set increases. Figure 8 shows the setting of 10-fold cross validation, where eight folds are employed for training, one for validation, and the rest for test. The confusion matrix of 10 trials were summed together, and then we reported the performance of current run. An ideal



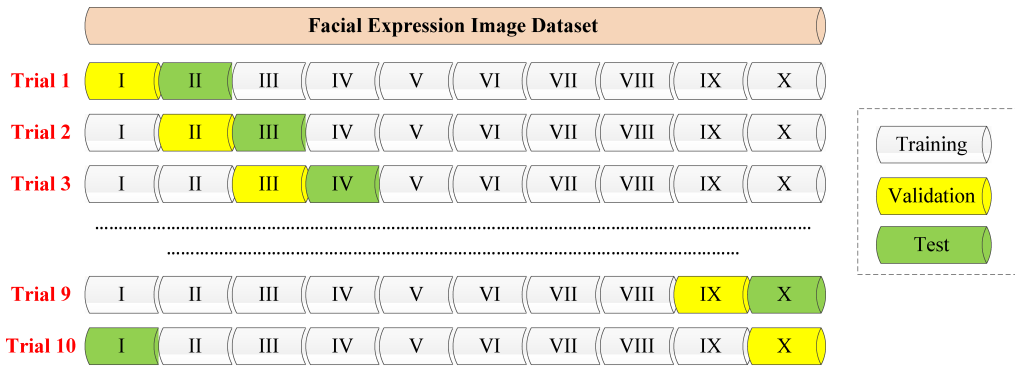


FIGURE 8. A run of 10-fold cross validation.

cost matrix  $\mathbb{C}$  is listed below:

$$\mathbb{C} = \begin{bmatrix} 100 & 0 & 0 & 0 & 0 & 0 & 0 \\ 0 & 100 & 0 & 0 & 0 & 0 & 0 \\ 0 & 0 & 100 & 0 & 0 & 0 & 0 \\ 0 & 0 & 0 & 100 & 0 & 0 & 0 \\ 0 & 0 & 0 & 0 & 100 & 0 & 0 \\ 0 & 0 & 0 & 0 & 0 & 100 & 0 \\ 0 & 0 & 0 & 0 & 0 & 0 & 100 \end{bmatrix} \quad (25)$$

which means all classes are identified correctly for the seven classes if there is a perfect classifier. In real condition, the classifier shall make mistakes, hence, we measure the classifier by the sensitivity (SEN) of each class. Suppose  $\mathbb{C} = [C_{ij}]$ ,  $i \in [1, 2, \dots, 7], j \in [1, 2, \dots, 7]$ , we defined the sensitivity of Class  $k$  as

$$SEN(k) = \frac{C_{kk}}{\sum_j C_{kj}} \quad (26)$$

Another important measure is the overall accuracy (OA) which is defined as

$$OA = \frac{\sum_i C_{ii}}{\sum_j \sum_i C_{ij}} \quad (27)$$

To further remove the randomness, we carried out the 10-fold stratified cross validation 10 runs. Each run, the fold segmentation was performed independently. In this way, we can report the mean and standard deviation of  $SEN(k)$  and OA.

## V. RESULTS AND DISCUSSIONS

### A. DWT VERSUS BWT

We used the center image in the first row in Figure 2 as an illustration. Figure 9(a-b) presents its 1-level, and 2-level DWT decomposition, respectively. For fair comparison, we used BWT decomposition over the same image, and the corresponding results are shown in Figure 10.

As we can observe from Figure 9 and Figure 10, both DWT and BWT can analyze original facial expression image in multi-scales, as the decomposition level increases. The higher the decomposition level is, the more detailed information

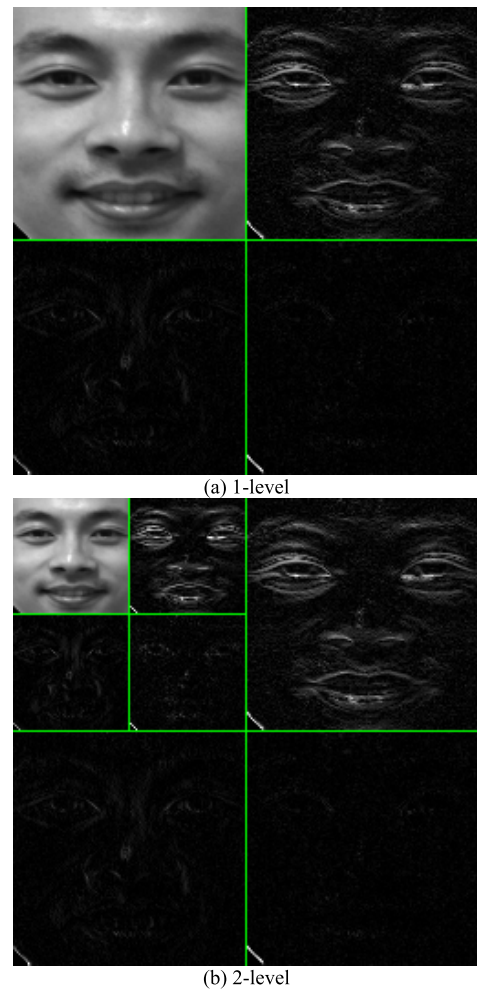


FIGURE 9. DWT result. (a) 1-level. (b) 2-level.

can be obtained. Nevertheless, the BWT subbands are more sparse than DWT, as shown in the  $C_h(1)$  and  $C_h(2)$  subbands, i.e., the 1-level and 2-level horizontal decomposition subbands. Other famous feature extraction techniques, such as Curve-like structure [43], [44], image moment [45] will be used in the future.

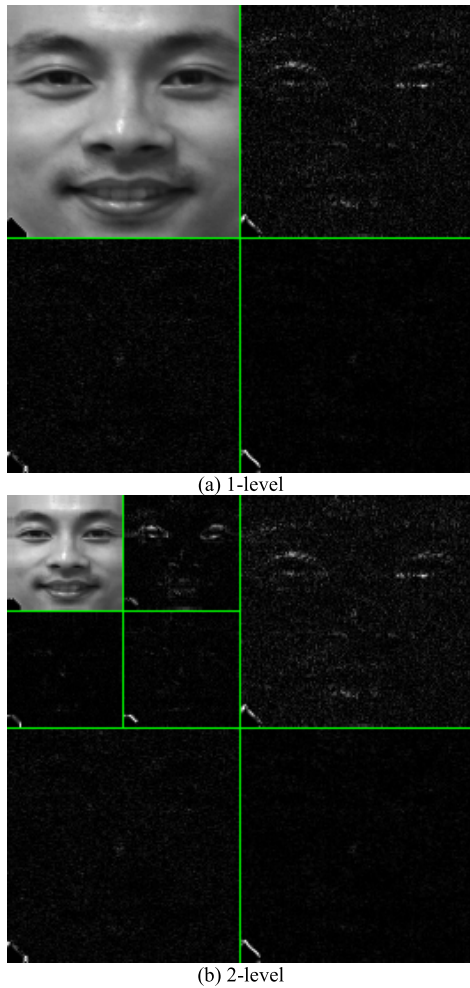


FIGURE 10. Biorthogonal wavelet transform result of the same image in Figure 9. (a) 1-level. (b) 2-level.

**B. STATISTICAL ANALYSIS**

The 10-fold stratified cross validation results are offered in Table 2. Here the sensitivities over anger, disgust, fear, happy, neutral, sadness, and surprise are  $98.00 \pm 1.08\%$ ,  $95.60 \pm 0.97\%$ ,  $96.10 \pm 0.99\%$ ,  $98.50 \pm 0.85\%$ ,  $97.30 \pm 0.70\%$ ,  $96.60 \pm 1.33\%$ , and  $95.30 \pm 1.64$ , respectively.

TABLE 2. Statistical analysis on the sensitivities of each class.

	Anger	Disgust	Fear	Happy	Neutral	Sadness	Surprise
Run 1	100.00	96.00	97.00	99.00	97.00	98.00	94.00
Run 2	99.00	95.00	95.00	99.00	97.00	97.00	97.00
Run 3	99.00	98.00	97.00	99.00	98.00	98.00	94.00
Run 4	98.00	96.00	96.00	97.00	97.00	99.00	97.00
Run 5	98.00	96.00	95.00	99.00	98.00	97.00	97.00
Run 6	97.00	98.00	97.00	98.00	97.00	97.00	96.00
Run 7	99.00	97.00	95.00	99.00	97.00	96.00	94.00
Run 8	100.00	96.00	97.00	99.00	99.00	94.00	93.00
Run 9	98.00	96.00	97.00	99.00	98.00	97.00	94.00
Run 10	97.00	97.00	95.00	97.00	98.00	97.00	97.00
Average	$98.00 \pm 1.08$	$95.60 \pm 0.97$	$96.10 \pm 0.99$	$98.50 \pm 0.85$	$97.30 \pm 0.70$	$96.60 \pm 1.33$	$95.30 \pm 1.64$

The results in Table 2 showed the sensitivities of Anger and Happy reach as high as  $98.00 \pm 1.08\%$  and  $98.50 \pm 0.85\%$ .

The facial emotion with third largest sensitivity is Neutral with average value of  $97.30 \pm 0.70$ . This result is in line with our initial guess.

First, the Anger facial expression is an intense emotional response when the person thought his/her personal boundaries are violated. Those people usually take following gestures: intense stare with eyes wide open, make sounds, bare the teeth, attempt to physically seem larger, etc. The staring with eyes wide open is a good indicator for both human and computers to identify Anger with other facial emotions. Indeed, there are other facial factors, such as V-shape eyebrows, wrinkled nose, narrowed eyes, forwarded jaws. All those predominant factors help to identify Anger emotion.

Second, the happiness represents an emotional state of well-being, based on emotions from contentment to delirious joy. In a happiness facial expression image, the reader can observe the forehead muscle relaxes and the eyebrows are pulled up slightly. Besides, both the wrinkled outer corners of eyes and pulled up lip corners are distinctive features. Calvo and Beltran [2] once used event-related potential (ERP) to demonstrate why Anger and Happiness are easily detected. Our results are coherent with their findings.

Third, the Neutral facial expression relaxes the facial muscles while other facial expression all need to use a massive of facial muscles. Ali et al. [13] got a perfect Neutral identification in their study. The reason is their dataset (Japanese Female Facial Expression) used professional models, who extensively and routinely used facial muscles in the daily life than common persons used in this study. Therefore, the other six facial expressions in their datasets seem more extreme than the expressions of our enrolled subjects.

TABLE 3. Statistical analysis on the overall accuracies.

Run	OA
1	96.71
2	96.71
3	96.86
4	96.71
5	96.86
6	96.86
7	96.57
8	96.86
9	96.71
10	96.86
Average	$96.77 \pm 0.10$

The overall accuracies of all runs are listed in Table 3. The final overall accuracy is  $96.77 \pm 0.10\%$ .

**C. CONFUSION MATRIX**

The confusion matrix of 10 runs are listed below in Table 4. Here the sum of each row equals to 1000, which represents the number of samples of each class (100) multiplied with the number of runs (10). Take the first row as an example, the data shows 980 Anger samples were correctly identified, and 10 Anger samples were misclassified as Disgust, 3 Anger samples were misclassified as Fear, 4 Anger samples were

misclassified as Happy, 2 Anger samples were misclassified as Sadness, and the left Anger sample was misclassified as Surprise.

TABLE 4. Confusion matrix over 10 runs.

	Anger	Disgust	Fear	Happy	Neutral	Sadness	Surprise
Anger	980	10	3	4	0	2	1
Disgust	28	956	6	1	2	5	2
Fear	5	4	961	0	7	4	19
Happy	1	1	4	985	3	2	4
Neutral	3	2	7	5	973	4	6
Sadness	10	8	6	2	0	966	8
Surprise	2	6	26	3	3	7	953

From Table 4, we can observe two important findings. One is Anger and Disgust are confused easily. The other is Fear and Surprise are confused easily. The reasons may result from the early phase of dynamic facial expressions between Anger and Disgust are similar due to the common transmission of nose wrinkle and lip funneler [46]. For Fear and Surprise, the upper lid raiser and jaw drop may contribute to the confusion [46]. Those two findings support the conclusion in [46].

TABLE 5. The effect of fuzzy logic in SVM.

	MSVM	FMSVM(Proposed)
Anger	95.10±1.32	98.00±1.08
Disgust	92.10±1.52	95.60±0.97
Fear	94.50±0.97	96.10±0.99
Happy	95.70±1.52	98.50±0.85
Neutral	94.90±1.10	97.30±0.70
Sadness	94.60±1.35	96.60±1.33
Surprise	94.50±0.97	95.30±1.64
OA	94.49±0.14	96.77±0.10

D. FMSVM VERSUS MSVM

In the fourth experiment, we shall test the effectiveness of fuzzy logic. We designed this experiment to compare our fuzzy multiclass SVM (FMSVM) classifier with multiclass SVM (MSVM). All the settings are the same as in Section V-B. The results are offered in Table 5.

We can observe from the data listed in Table 5, that the MSVM without fuzzy logic obtains lower sensitivities in all facial emotion classes and lower overall accuracy than the FMSVM with fuzzy logic. Therefore, this proves the effectiveness of using fuzzy logic.

E. COMPARISON TO STATE-OF-THE-ART APPROACHES

In the fifth experiment, we compared our proposed “BWE + FMSVM” method with three state-of-the-art methods over our dataset. The comparison basis methods include PCA + SVM [11], CSO-GA-PSO + SVM [12], and RT + HOS + SVM [13]. All the settings are the same as in Section V.B. The comparison results are listed in Table 6.

Table 6 shows the PCA + SVM [11] yields an overall accuracy of 89.14±2.91%, the CSO-GA-PSO + SVM [12] yields an overall accuracy of 93.86±0.39%, RT + HOS + SVM [13]

TABLE 6. Comparison to state-of-the-art methods.

Approach	OA
PCA + SVM [11]	89.14±2.91
CSO-GA-PSO + SVM [12]	93.86±0.39
RT + HOS + SVM [13]	83.43±2.15
BWE + FMSVM (Proposed)	96.77±0.10

yields an overall accuracy of 83.43±2.15%, and our method yields the largest overall accuracy of 96.77±0.10%.

Although our develop FER system achieved promising results and performed better than three state-of-the-art approaches, it yet had several shortcomings: (i) we did not consider the geometric transform of faces, such as yaw angles [47]. (ii) We used still image, not video images [48].

In the future, we may use apply our system to help treat and diagnosis patients with emotion problems: Luzzi et al. [49] once requested AD patients to identify happy/sad to measure their disease. Chen et al. [50] also used facial expression to improve perceptions and judgments of autism children. We believed our system can help quantitatively measure the emotional identification ability of AD [51]–[55] and autism [56] patients. Besides, more advanced image processing [57] techniques, artificial intelligence [58], [59] approaches, and swarm intelligence [60], [61] methods shall be tested. Our method can apply to not only facial expression images, but also MR images [62], [63], CT images, remote-sensing images [64], [65], etc.

VI. CONCLUSION

In this study, we proposed a new facial emotion recognition system based on facial expression image. Our methodology chose the biorthogonal wavelet entropy and fuzzy multiclass support vector machine. The strict statistical analysis showed the superiority of our method to other three state-of-the-art methods. In the future, we shall apply our method in recommender system [66], [67], cloud computing [68], big data [69]. Sparse representation [70] is another potential research direction.

VII. CONFLICT OF INTEREST

We have no conflict of interest to disclose, with regard to the subject matter of this paper.

REFERENCES

- [1] S. Bernaerts, E. Berra, N. Wenderoth, and K. Alaerts, “Influence of oxytocin on emotion recognition from body language: A randomized placebo-controlled trial,” *Psychoneuroendocrinology*, vol. 72, pp. 182–189, Oct. 2016.
- [2] M. G. Calvo and D. Beltrán, “Brain lateralization of holistic versus analytic processing of emotional facial expressions,” *NeuroImage*, vol. 92, pp. 237–247, May 2014.
- [3] C. M. Jones and I.-M. Jonsson, “Performance analysis of acoustic emotion recognition for in-car conversational interfaces,” in *Proc. 4th Int. Conf. Universal Access Human-Comput. Interact.*, Beijing, China, 2007, pp. 411–420.
- [4] R. Jenke, A. Peer, and M. Buss, “Feature extraction and selection for emotion recognition from EEG,” *IEEE Trans. Affect. Comput.*, vol. 5, no. 3, pp. 327–339, Jul/Sep. 2014.

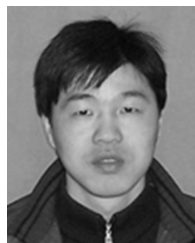


- [5] S. Senecal, L. Cuel, A. Aristidou, and N. Magnenat-Thalmann, "Continuous body emotion recognition system during theater performances," *Comput. Animation Virtual Worlds*, vol. 27, nos. 3–4, pp. 311–320, May/Aug. 2016.
- [6] S. Lalitha, A. Mudupu, B. V. Nandyala, and R. Munagala, "Speech emotion recognition using DWT," in *Proc. Int. Conf. Comput. Intell. Comput. Res.*, Madurai, India, Dec. 2015, pp. 20–23.
- [7] D. J. Martino, C. Samamé, and S. A. Strejilevich, "Stability of facial emotion recognition performance in bipolar disorder," *Psychiatry Res.*, vol. 243, pp. 182–184, Sep. 2016.
- [8] H. Memisevic, E. Mujkanovic, and I. Ibralic-Biscevic, "Facial emotion recognition in adolescents with disabilities: The effects of type of disability and gender," *Perceptual Motor Skills*, vol. 123, pp. 127–137, Aug. 2016.
- [9] J. Pietschnig et al., "Facial emotion recognition and its relationship to cognition and depressive symptoms in patients with Parkinson's disease," *Int. Psychogeriatrics*, vol. 28, no. 7, pp. 1165–1179, Jul. 2016.
- [10] S. Argaud et al., "Does facial amimia impact the recognition of facial emotions? An EMG study in Parkinson's disease," *PLoS ONE*, vol. 11, Jul. 2016, Art. no. e0160329.
- [11] D. Drume and A. S. Jalal, "A multi-level classification approach for facial emotion recognition," in *Proc. Int. Conf. Comput. Intell. Comput. Res.*, Coimbatore, India, Dec. 2012, pp. 288–292.
- [12] T. V. Vivek and G. R. M. Reddy, "A hybrid bioinspired algorithm for facial emotion recognition using CSO-GA-PSO-SVM," in *Proc. 5th Int. Conf. Commun. Syst. Netw. Technol.*, Gwalior, India, Apr. 2015, pp. 472–477.
- [13] H. Ali, M. Hariharan, S. Yaacob, and A. H. Adom, "Facial emotion recognition based on higher-order spectra using support vector machines," *J. Med. Imag. Health Informat.*, vol. 5, no. 6, pp. 1272–1277, Oct. 2015.
- [14] T. Takehara, F. Ochiai, and N. Suzuki, "A small-world network model of facial emotion recognition," *Quart. J. Experim. Psychol.*, vol. 69, pp. 1508–1529, Aug. 2016.
- [15] M. Alhussein, "Automatic facial emotion recognition using weber local descriptor for e-Healthcare system," *Cluster Comput.-J. Netw. Softw. Tools Appl.*, vol. 19, no. 1, pp. 99–108, Mar. 2016.
- [16] F. Y. Shih and C.-F. Chuang, "Automatic extraction of head and face boundaries and facial features," *Inf. Sci.*, vol. 158, pp. 117–130, Jan. 2004.
- [17] R. C. Guido, "Practical and useful tips on discrete wavelet transforms [sp tips & tricks]," *IEEE Signal Process. Mag.*, vol. 32, no. 3, pp. 162–166, May 2015.
- [18] H. N. Alves and R. N. B. Fonseca, "An algorithm based on discrete wavelet transform for fault detection and evaluation of the performance of overcurrent protection in radial distribution systems," *IEEE Latin Amer. Trans.*, vol. 12, no. 4, pp. 602–608, Jun. 2014.
- [19] W. Schnurrer, T. Tröger, T. Richter, J. Seiler, and A. Kaup, "Efficient lossless coding of highpass bands from block-based motion compensated wavelet lifting using JPEG 2000," in *Proc. Vis. Commun. Image Process. Conf.*, Valletta, Malta, Dec. 2014, pp. 398–401.
- [20] M. Chen et al., "Detection of dendritic spines using wavelet-based conditional symmetric analysis and regularized morphological shared-weight neural networks," *Comput. Math. Methods Med.*, vol. 2015, Sep. 2015, Art. no. 454076, doi: 10.1155/2015/454076.
- [21] J. Kim, "Discrete wavelet transform-based feature extraction of experimental voltage signal for li-ion cell consistency," *IEEE Trans. Veh. Technol.*, vol. 65, no. 3, pp. 1150–1161, Mar. 2016.
- [22] E. A. Junior, R. A. D. M. Valentim, and G. B. Brandao, "Real time QRS detection based on redundant discrete wavelet transform," *IEEE Latin Amer. Trans.*, vol. 14, no. 4, pp. 1662–1668, Apr. 2016.
- [23] Y. C. Guo, L. L. Hu, and R. Ding, "Orthogonal wavelet transform weighted multi-modulus blind equalization algorithm based on quantum particle swarm optimization," *Acta Phys. Sin.*, vol. 61, Mar. 2012, Art. no. 054304.
- [24] X.-G. Zhu, B.-B. Li, and D.-F. Li, "Orthogonal wavelet transform of signal based on complex B-spline bases," *Int. J. Wavelets Multiresolution Inf. Process.*, vol. 10, no. 6, Nov. 2012, Art. no. 1250054.
- [25] H. Sun, J. Wang, and R. Shao, "Depressing defocusing effect in microscopy by bi-orthogonal wavelet transform," *Particuology*, vol. 10, no. 5, pp. 644–647, Oct. 2012.
- [26] O. Prakash and A. Khare, "Tracking of moving object using energy of biorthogonal wavelet transform," *Chiang Mai J. Sci.*, vol. 42, no. 3, pp. 783–795, Jul. 2015.
- [27] K. H. Norwich, "Boltzmann–Shannon entropy and the double-slit experiment," *Phys. A, Statist. Mech. Appl.*, vol. 462, pp. 141–149, Nov. 2016.
- [28] W. S. Nascimento and F. V. Prudente, "Study of Shannon entropy in the context of quantum mechanics: An application to free and confined harmonic oscillator," *Quimica Nova*, vol. 39, no. 6, pp. 757–764, Jul. 2016.
- [29] Y. Zhang and L. Wu, "An MR brain images classifier via principal component analysis and kernel support vector machine," *Prog. Electromagn. Res.*, vol. 130, pp. 369–388, Sep. 2012.
- [30] J. Behmann, K. Hendriksen, U. Müller, W. Büscher, and L. Plümer, "Support vector machine and duration-aware conditional random field for identification of spatio-temporal activity patterns by combined indoor positioning and heart rate sensors," *Geoinformatica*, vol. 20, no. 4, pp. 693–714, Jan. 2016.
- [31] Y. Zhang, S. Wang, and Z. Dong, "Classification of Alzheimer disease based on structural magnetic resonance imaging by kernel support vector machine decision tree," *Prog. Electromagn. Res.*, vol. 144, pp. 171–184, 2014.
- [32] F. Ali, K.-S. Kwak, and Y.-G. Kim, "Opinion mining based on fuzzy domain ontology and support vector machine: A proposal to automate online review classification," *Appl. Soft Comput.*, vol. 47, pp. 235–250, Oct. 2016.
- [33] X.-X. Zhou et al., "Comparison of machine learning methods for stationary wavelet entropy-based multiple sclerosis detection: Decision tree,  $k$ -nearest neighbors, and support vector machine," *Simulation*, vol. 92, pp. 861–871, Sep. 2016.
- [34] T. Genewein and D. A. Braun, "Bio-inspired feedback-circuit implementation of discrete, free energy optimizing, winner-take-all computations," *Biological*, vol. 110, no. 2, pp. 135–150, Jun. 2016.
- [35] Y. Zhang and L. Wu, "Classification of fruits using computer vision and a multiclass support vector machine," *Sensors*, vol. 12, no. 9, pp. 12489–12505, 2012.
- [36] M. Kim and C. M. Twigg, "Rank determination by winner-take-all circuit for rank modulation memory," *IEEE Trans. Circuits Syst. II, Express Briefs*, vol. 63, no. 4, pp. 326–330, Apr. 2016.
- [37] Y. Chen et al., "Pathological brain detection by wavelet-energy and fuzzy support vector machine," in *Proc. 8th Int. Symp. Comput. Intell. Design (ISCID)*, Hangzhou, China, Dec. 2015, pp. 409–412.
- [38] G. Liu et al., "Pathological brain detection in MRI scanning by wavelet packet Tsallis entropy and fuzzy support vector machine," *SpringerPlus*, vol. 4, Nov. 2015, Art. no. 716.
- [39] A. Khormali and J. Addeh, "A novel approach for recognition of control chart patterns: Type-2 fuzzy clustering optimized support vector machine," *ISA Trans.*, vol. 63, pp. 256–264, Jul. 2016.
- [40] J. Yang, S. Wang, Y. Zhang, P. Phillips, J. Yang, and T.-F. Yuan, "Identification of green, oolong and black teas in China via wavelet packet entropy and fuzzy support vector machine," *Entropy*, vol. 17, no. 10, pp. 6663–6682, 2015.
- [41] H. Samma, C. P. Lim, J. M. Saleh, and S. A. Suandi, "A memetic-based fuzzy support vector machine model and its application to license plate recognition," *Memetic Comput.*, vol. 8, no. 3, pp. 235–251, Sep. 2016.
- [42] U. Ekong et al., "Classification of epilepsy seizure phase using interval type-2 fuzzy support vector machines," *Neurocomputing*, vol. 199, pp. 66–76, Jul. 2016.
- [43] Y. Chen et al., "Curve-like structure extraction using minimal path propagation with backtracking," *IEEE Trans. Image Process.*, vol. 25, no. 2, pp. 988–1003, Feb. 2016.
- [44] Y. Chen et al., "Structure-adaptive fuzzy estimation for random-valued impulse noise suppression," *IEEE Trans. Circuits Syst. Video Technol.*, pp. 1–11, Oct. 2016, doi: 10.1109/TCSVT.2016.2615444.
- [45] P. Sun, Y. Zhang, S. Wang, and P. Phillips, "Pathological brain detection based on wavelet entropy and Hu moment invariants," *Bio-Med. Mater. Eng.*, vol. 26, no. S1, pp. S1283–S1290, 2015.
- [46] R. E. Jack, O. G. B. Garrod, and P. G. Schyns, "Dynamic facial expressions of emotion transmit an evolving hierarchy of signals over time," *Current Biol.*, vol. 24, no. 2, pp. 187–192, Jan. 2014.
- [47] D. KrishnaSri, P. Suja, and S. Tripathi, "Emotion recognition from 3D images with non-frontal view using geometric approach," in *Advances in Signal Processing and Intelligent Recognition Systems*, vol. 425, S. M. Thampi, S. Bandyopadhyay, S. Krishnan, K.-C. Li, S. Mosin, and M. Ma, Eds. Berlin, Germany: Springer-Verlag, 2016, pp. 63–73.
- [48] V. P. K. Kumar, P. Suja, and S. Tripathi, "Emotion recognition from facial expressions for 4D videos using geometric approach," in *Advances in Signal Processing and Intelligent Recognition Systems*, vol. 425, S. M. Thampi, S. Bandyopadhyay, S. Krishnan, K.-C. Li, S. Mosin, and M. Ma, Eds. Berlin, Germany: Springer-Verlag, 2016, pp. 3–14.
- [49] S. Luzzi, M. Piccirilli, and L. Provinciali, "Perception of emotions on happy/sad chimeric faces in Alzheimer disease: Relationship with cognitive functions," *Alzheimer Disease Assoc. Disorders*, vol. 21, no. 2, pp. 130–135, Apr./Jun. 2007.

- [50] C.-H. Chen, I.-J. Lee, and L.-Y. Lin, "Augmented reality-based video-modeling storybook of nonverbal facial cues for children with autism spectrum disorder to improve their perceptions and judgments of facial expressions and emotions," *Comput. Human Behavior*, vol. 55, pp. 477–485, Feb. 2016.
- [51] T.-F. Yuan et al., "Detection of subjects and brain regions related to Alzheimer's disease using 3D MRI scans based on eigenbrain and machine learning," *Frontiers Comput. Neurosci.*, vol. 9, Jun. 2015, Art. no. 66.
- [52] P. Phillips, Z. Dong, G. Ji, J. Yang, Y. Zhang, and S. Wang, "Detection of Alzheimer's disease and mild cognitive impairment based on structural volumetric MR images using 3D-DWT and WTA-KSVM trained by PSOTVAC," *Biomed. Signal Process. Control*, vol. 21, pp. 58–73, Aug. 2015.
- [53] Y. Zhang and S. Wang, "Detection of Alzheimer's disease by displacement field and machine learning," *PeerJ*, vol. 3, Sep. 2015, Art. no. e1251.
- [54] G. Liu, P. Phillips, T.-F. Yuan, S. Wang, and Y. Zhang, "Detection of Alzheimer's disease by three-dimensional displacement field estimation in structural magnetic resonance imaging," *J. Alzheimer's Disease*, vol. 50, no. 1, pp. 233–248, Oct. 2016.
- [55] P. Phillips, Y. Zhang, P. Phillips, J. Yang, and T.-F. Yuan, "Three-dimensional eigenbrain for the detection of subjects and brain regions related with Alzheimer's disease," *J. Alzheimer's Disease*, vol. 50, no. 4, pp. 1163–1179, 2016.
- [56] S. Goh, Z. Dong, Y. Zhang, S. DiMauro, and B. S. Peterson, "Mitochondrial dysfunction as a neurobiological subtype of autism spectrum disorder: Evidence from brain imaging," *JAMA Psychiatry*, vol. 71, no. 6, pp. 665–671, 2014.
- [57] B. Peng et al., "Image processing methods to elucidate spatial characteristics of retinal microglia after optic nerve transection," *Sci. Rep.*, vol. 6, Feb. 2016, Art. no. 21816.
- [58] S. Balochian, "Artificial intelligence and its applications," in *Mathematical Problems in Engineering*. USA: Hindawi Publishing Corporation, 2014, Art. no. 840491.
- [59] P. Agarwal, "Artificial intelligence and its applications 2014," in *Mathematical Problems in Engineering*. USA: Hindawi Publishing Corporation, 2016, Art. no. 3871575, doi: 10.1155/2016/3871575.
- [60] Y. Zhang, P. Agarwal, V. Bhatnagar, S. Balochian, and J. Yan, "Swarm intelligence and its applications," *Sci. World J.*, vol. 2013, Sep. 2013, Art. no. 528069.
- [61] P. Agarwal, V. Bhatnagar, S. Balochian, Y. Zhang, and X. Zhang, "Swarm intelligence and its applications 2014," in *Sci. World J.*, Sep. 2014, Art. no. 204294.
- [62] L. Wu, Y. Zhang, Z. Dong, and S. Wang, "A hybrid method for MRI brain image classification," *Expert Syst. Appl.*, vol. 38, no. 8, pp. 10049–10053, Aug. 2011.
- [63] L. Wu, Y. Zhang, and S. Wang, "Magnetic resonance brain image classification by an improved artificial bee colony algorithm," *Prog. Electromagn. Res.*, vol. 116, pp. 65–79, Jun. 2011.
- [64] L. Wu and Y. Zhang, "Crop classification by forward neural network with adaptive chaotic particle swarm optimization," *Sensors*, vol. 11, no. 5, pp. 4721–4743, 2011.
- [65] N. Neggaz, G. Wei, Y. Zhang, and S. Wang, "Remote-sensing image classification based on an improved probabilistic neural network," *Sensors*, vol. 9, no. 9, pp. 7516–7539, 2009.
- [66] Y. Zhang, "GroRec: A group-centric intelligent recommender system integrating social, mobile and big data technologies," *IEEE Trans. Serv. Comput.*, vol. 9, no. 5, pp. 786–795, Sep./Oct. 2016.
- [67] Y. Zhang, M. Chen, D. Huang, D. Wu, and Y. Li, "iDoctor: Personalized and professionalized medical recommendations based on hybrid matrix factorization," *Future Generat. Comput. Syst.*, vol. 66, pp. 30–35, Jan. 2017.
- [68] Y. Baimbetov, I. Khalil, M. Steinbauer, and G. Anderst-Kotsis, "Using big data for emotionally intelligent mobile services through multi-modal emotion recognition," in *Inclusive Smart Cities and E-Health*, vol. 9102, A. Geissbühler, J. Demongeot, M. Mokhtari, B. Abdulrazak, and H. Aloulou, Eds. Berlin, Germany: Springer-Verlag, 2015, pp. 127–138.
- [69] Y. Zhang, M. Chen, S. Mao, L. Hu, and V. Leung, "CAP: Community activity prediction based on big data analysis," *IEEE Netw.*, vol. 28, no. 4, pp. 52–57, Jul./Aug. 2014.
- [70] L. Shi et al., "Corrigendum: Improving low-dose cardiac CT images based on 3D sparse representation," *Sci. Rep.*, vol. 6, Mar. 2016, Art. no. 22804.



image processing.



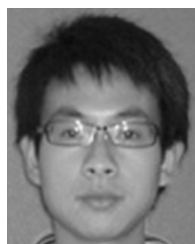
**YU-DONG ZHANG** received the Ph.D. degree in signal and information processing from Southeast University in 2010. From 2010 to 2012, he held a post-doctoral position with Columbia University. From 2012 to 2013, he was an Assistant Research Scientist with Columbia University. He is currently a Full Professor and a Ph.D. Advisor with the School of Computer Science and Technology, Nanjing Normal University. His research interests focus on computer-aided diagnosis and biomedical

**ZHANG-JING YANG** received the B.Sc. degree in computer science and education from Nanjing Normal University in 2004, and the M.Sc. and Ph.D. degrees in computer applications from the Nanjing University of Science and Technology, China, in 2010 and 2014, respectively. He is currently with the School of Technology, Nanjing Audit University. His current interests are in the areas of pattern recognition, computer vision, and machine learning.



His current research interests include computer vision, robotics, artificial intelligence, and ocean observing.

**HUI-MIN LU** received the B.S. degree in electronics information science and technology from Yangzhou University in 2008, the M.S. degrees in electrical engineering from the Kyushu Institute of Technology and Yangzhou University in 2011, and the Ph.D. degree in electrical engineering from the Kyushu Institute of Technology in 2014. He is currently an Associate Professor with the Kyushu Institute of Technology. He also serves as an Excellent Young Researcher of MEXT-Japan.



**XING-XING ZHOU** is currently pursuing the Ph.D. degree with Nanjing Normal University. His research interest is biomedical image processing.

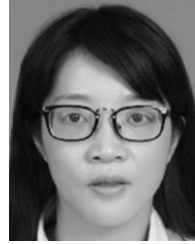


Marshall University in 2016. She has also conducted research on using magnetic resonance spectroscopy in diagnosing panic disorder at the Columbia Presbyterian Medical Center. She has also helped conduct research analyzing pain mechanisms in rats at Stony Brook University.

**PREETHA PHILLIPS** received the B.Sc. degree from Shepherd University in 2016. She is currently pursuing the Ph.D. degree in osteopathic medicine with the West Virginia School of Osteopathic Medicine. She has conducted research in Shepherd University in investigating the effects of Roundup on the sex hormones in the aquatic snail, *Lymnaea palustris*. She received an honorable mention for a poster presentation for this research in the West Virginia Academy of Science that took place at



**QING-MING LIU** is currently pursuing the Ph.D. degree with the School of Psychology, Nanjing Normal University, China. His research interest is consciousness, addiction, and sleep.



**SHUI-HUA WANG** received the B.S. degree from Southeast University in 2008, the M.S. degree from The City University of New York in 2012, and the Ph.D. degree from Nanjing University in 2016. She is currently an Assistant Professor with Nanjing Normal University.

...